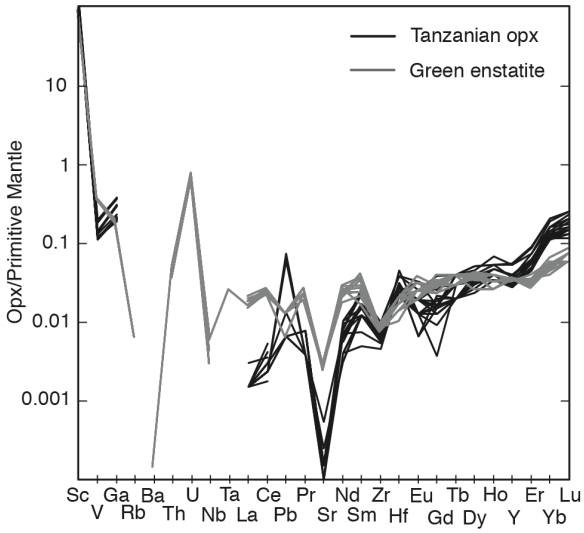

Fig. B1: Trace element contents of the Tanzanian orthopyroxene and the green enstatite normalized to primitive mantle.

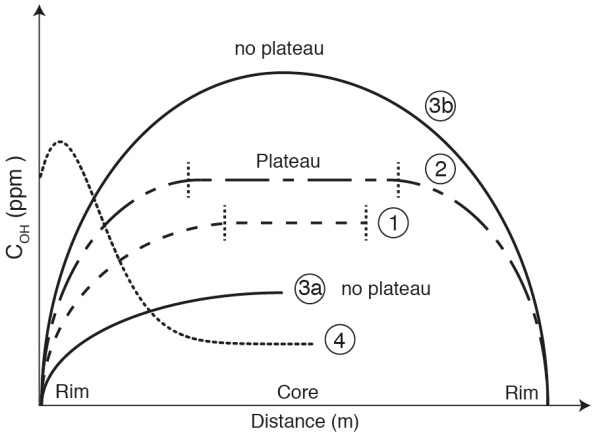

Fig. B2: The 4 different diffusion profile shapes encountered in this study. 1) half a profile including a plateau (Eq. 2); 2) is a full profile including a plateau (Eq. 3); 3a) and 3b) show half and full profiles which are numerically solved, 4) is half a profile with D approximated by Eq. 1. 1) and 2) are solved analytically.

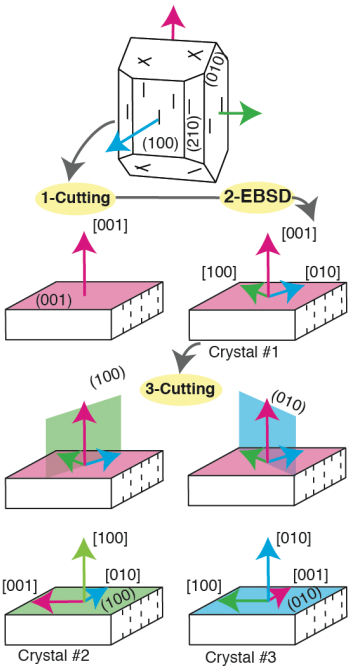

Fig. B3: Cutting and orienting process. The crystal is first cut along (001). The orientation was verified by EBSD and the [100] and [010] axes were positioned on (001). The initial crystal was cut in two pieces with the position of [100] and [010] respectively. They were then cut to obtain (100) and (010).

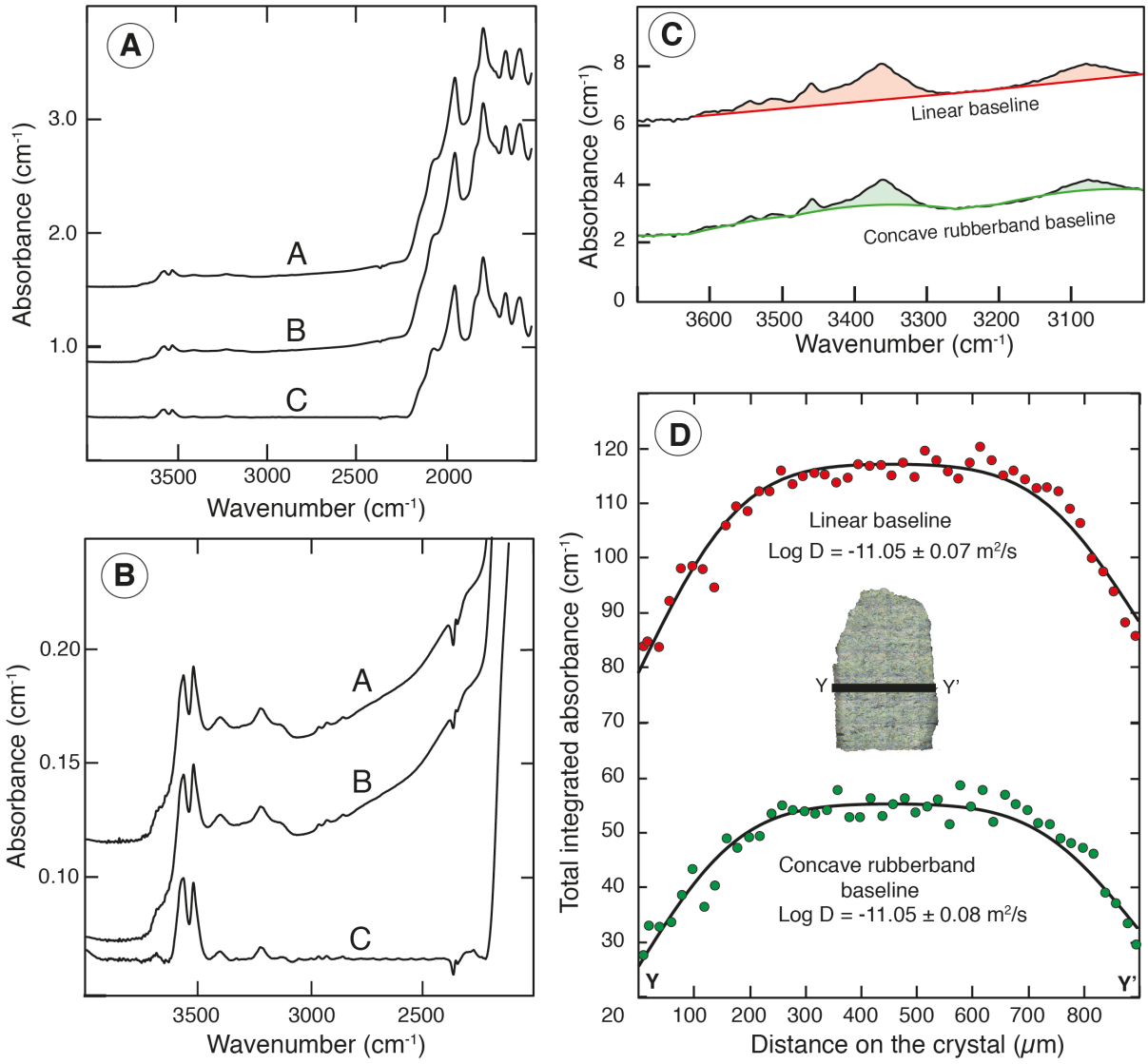

Fig. B4: Baseline corrections comparison. A) and B) Comparison between mantle orthopyroxene FTIR spectra to show the effect of the atmospheric and baseline corrections. The rubberband tool is used to remove any potential contribution from H_2O. A - raw spectrum (no correction), B - Atmosphere corrected, C - atmosphere and baseline corrected (concave rubberband tool, 64 baseline points, 3 iterations). In A) spectra shown for wavenumbers between 1500 cm^{-1} to 4000 cm^{-1} and in B) spectra shown for wavenumbers between 2000 cm^{-1} to 4000 cm^{-1}. C) Comparison between the integrated area in the FTIR OH stretching region of the Tanzanian orthopyroxene using a linear baseline and a concave rubberband baseline (what is used in this study). D) Comparison between the total integrated absorbance profile across an experiment crystal (914°C, ol-opx buffer, ~ΔQFM-1, 20 minutes) using the linear and concave rubberband baselines shown in C). Diffusion coefficients for both were calculated using an analytical solution (Eq.3) to Fick's second law (Eq.1). The total integrated absorbance is larger using a linear baseline than with a concave rubberband baseline, but they yield the same diffusion coefficients. The water contents are underestimated with the concave rubberband baseline.

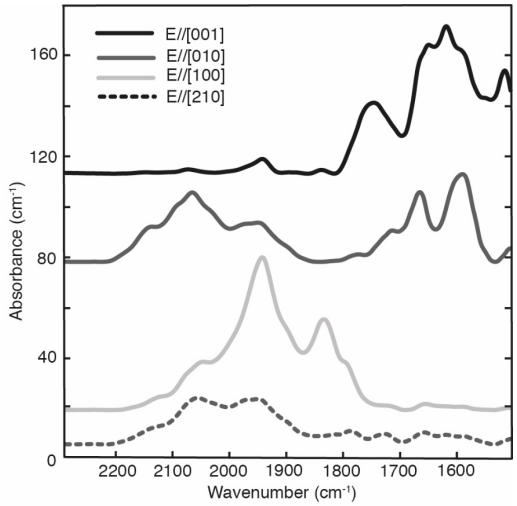

Fig. B5: Stacked FTIR spectra of the Si-overtone region (1500-2300 cm^{-1}) of the Tanzanian opx starting material for E//[001], E//[010], E//[001] and E//[210].

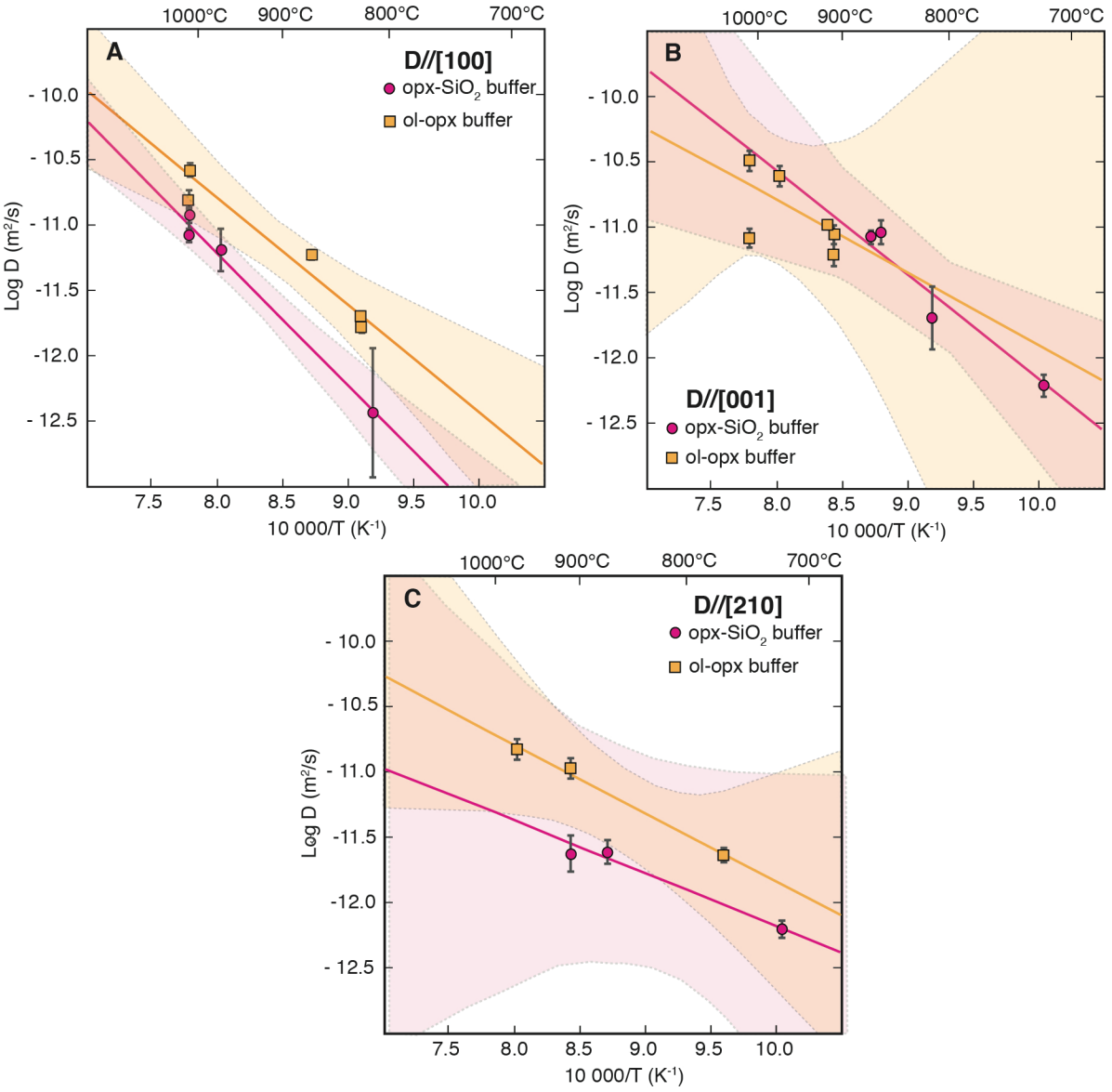

Fig. B6: Arrhenius diagram of hydrogen diffusivities of the Tanzanian orthopyroxene comparing the effect of the ol-opx and opx-SiO_2 buffers, for A) D//[100], B) D/[210| and C) D//[001]. The solid lines show the calculated weighted linear regression for the ol-opx buffer diffusivities (orange) and for the opx-SiO_2 buffer diffusivities (pink). The shaded areas are show the 95% confidence envelopes for ol-opx buffer diffusivities (orange) and for the opx-SiO_2 buffer diffusivities (pink). The diagram of D//[010] is not shown due to the too few data points for each buffers to make a relevant confidence envelope.

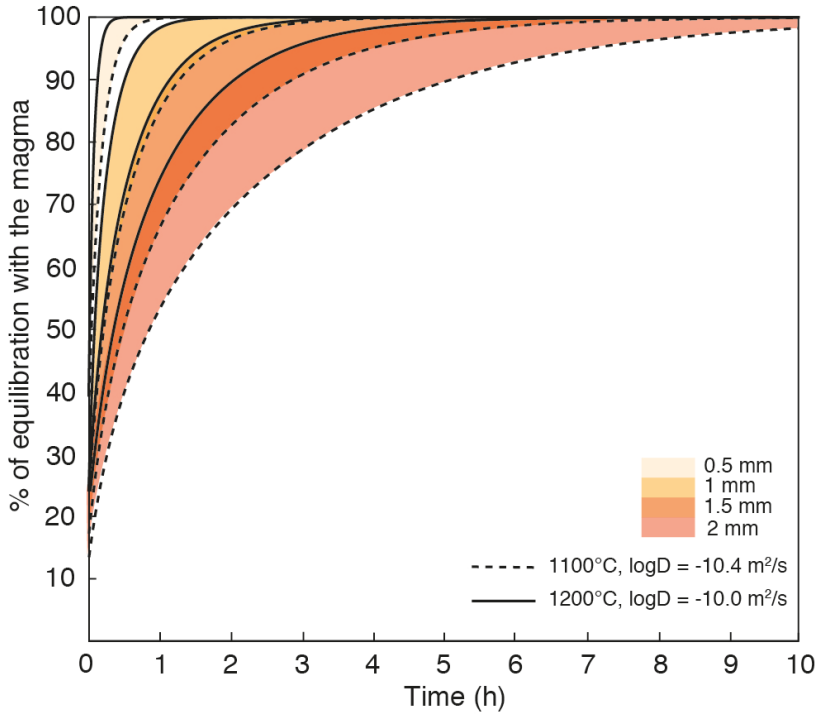

Fig.B7 : Hydrogen re-equilibration, at 1100 °C and 1200 °C, between the host-magma and spherical orthopyroxene crystals with a radius R, presented as a function of time, with different radius ranging from 0.5 mm to 2 mm. The calculations are based on the analytical solution of Fick's second law (Eq.1) for a spherical geometry of radius R (Crank, 1979, Eq 6.20). D//[010] at 1100°C and 1200°C from this study were used for the calculations.